Rapid synthesis of mesoporous TiO_2 with high photocatalytic activity by ultrasound-induced agglomeration

Jimmy C. Yu,* Lizhi Zhang and Jiaguo Yu

Department of Chemistry and Environmental Science Programme, The Chinese University of Hong Kong, Shatin, New TerritoriesHong Kong. E-mail: jimyu@cuhk.edu.hk

Received (in London, UK) 9th October 2001, Accepted 25th October 2001
First published as an Advance Article on the web 26th February 2002

Three-dimensional and thermally stable mesoporous TiO_2 was synthesized without the use of any surfactants *via* treatment with high intensity ultrasound irradiation for a short period of time. Monodispersed TiO_2 sol particles were formed initially by ultrasound-assisted hydrolysis of acetic acid-modified titanium isopropoxide. Then, the mesoporous spherical or globular particles, which have a narrow pore size distribution, were produced by controlled condensation and agglomeration of these sol nanoparticles under high intensity ultrasound irradiation. The mesoporous TiO_2 was characterized by XRD, TEM, nitrogen adsorption, TGA/DTA and FTIR. Low-angle XRD and TEM show the mesoporous TiO_2 has a wormhole-like structure and a lack of long-range order. Nitrogen adsorption results indicate that the mesoporous TiO_2 retains mesoporosity with a narrow pore size distribution and high surface area to at least 673 K. The thermal stability of mesoporous TiO_2 is attributed to its thick inorganic walls, consisting of TiO_2 nanoparticles. TGA study shows that this synthetic method is environmentally friendly. The photocatalytic activity of mesoporous TiO_2 for the oxidation of acetone in air was measured. As-prepared mesoporous TiO_2 has negligible activity due to its amorphous structure. Calcined mesoporous TiO_2 shows better activity than commercial photocatalyst P25. The reasons for the high activity of mesoporous TiO_2 are discussed.

Introduction

Since the discovery of the M41S family of ordered mesoporous molecular sieves, utilizing electrostatic interactions between a positively charged surfactant (S^+) and a negatively charged inorganic precursor (I^-), by Mobil in 1992,[1] a variety of ordered mesoporous materials have been synthesized using ionic or neutral surfactants as templates through different assembly pathways.[1–3] All the ionic pathways are based on the charge matching between the ionic surfactants and the precursors through electrostatic interactions. Hydrogen bonding or covalent bonds between neutral surfactants and the precursors are suggested to direct the formation of the mesostructures during neutral pathways. Recently, Wei and coworkers developed a non-surfactant templating method to synthesize mesoporous silica by using non-surfactant organic compounds as templates or pore forming agents.[4–6] In that study, the pore diameter was controlled between ~2 and 6 nm by varying the template concentration. Besides using micelles and very large and complex organic molecules, Jansen *et al.* recently found that small organic molecules such as triethanolamine could also be used as templates to synthesize mesoporous silica (TUD-1) with a three-dimensional network.[7] However, all these pathways require removal of these templates by extraction and/or calcination to obtain the final products, which may cause the collapse of the framework of mesoporous materials and could also generate environmental pollution. Furthermore, materials synthesized with non-surfactant templating methods are limited to silica.

Titanium dioxide is well known as a large-bandgap semiconductor with high photocatalytic activity.[8] Since Antonelli and Ying reported a modified sol–gel synthesis of hexagonally packed mesoporous TiO_2 in 1995, mesoporous TiO_2 has attracted much attention because of its high surface area and large, uniform pores, which are of great importance in catalysis and solar cell applications.[2] Many kinds of mesoporous TiO_2 have been synthesized through conventional approaches using surfactants as templates.[2,9,10] Sonochemical processing has been proven to be a useful technique to synthesize novel materials with unusual properties.[11,12] The conventional synthesis of mesoporous TiO_2 needs several days or longer. Recently, Wang *et al.* reported a sonochemical synthesis of mesoporous TiO_2 with wormhole-like framework structures using a long-chain amine as the structure-directing agent and titanium isopropoxide (TIP) as the precursor,[13] shortening the synthesis time considerably. However, the mesoporous structure is only stable to about 523 K and starts to disintegrate at 573 K; it is also time-consuming to remove the surfactant with an appropriate solvent. On the other hand, only mesoporous anatase with a broad pore size distribution was obtained if TIP was directly injected into deionized water in the sonication cell under continuous sonication without using any surfactants.[14] The authors attributed the formation of mesoporous structures to the aggregation of particles. It is clear that the rate of hydrolysis is too fast for the formation of uniformly sized sol particles. Thus, a narrow pore size distribution could not be obtained. Herein, we report a novel rapid approach to the synthesis of highly active, three-dimensional, thermally stable mesoporous TiO_2 under ultrasound irradiation without the use of a template. We employed acetic acid as a modifying agent to slow down the rate of hydrolysis, and the desired thermally stable mesoporous TiO_2 (SMT, AP denotes as-prepared SMT, and the number indicates the calcination temperature) with wormhole-like framework structures and a narrow pore size distribution was obtained. This approach is based on a new idea that the controlled condensation and agglomeration of monodispersed sol particles would lead to the formation of a mesoporous structure with a narrow

 DOI: 10.1039/b109173e

pore size distribution under high intensity ultrasound irradiation, which we call ultrasound-induced agglomeration (UIA).

Results and discussion

X-Ray diffraction analysis

The low-angle powder X-ray diffraction (XRD) patterns of the as-prepared and calcined SMT are shown in the inset of Fig. 1. A distinctive peak with a *d*-spacing of 13 nm appears in the sample calcined at 673 K (SMT-673), indicating that SMT has good thermal stability and a robust framework. Wang *et al*. observed a single broad peak in the low-angle XRD spectrum of their mesoporous TiO_2 prepared with templates under ultrasound irradiation.[13] However, the peak disappeared after calcination at 623 K due to the collapse of the framework. Analogous single peak patterns corresponding to a large *d*-spacing have also been reported for disordered MCM-41,[15,16] HMS[3] and MSU-X.[3] The intensities of the XRD peak are substantially stronger for SMT-673 than for SMT-AP. Similar differences in XRD intensities have also been observed for MCM-41 and HMS.[3] According to the wide-angle XRD patterns for SMT shown in Fig. 1, SMT-AP has an amorphous structure. After calcination at 673 K, SMT-AP is converted to the anatase form with a crystallite size of about 8.6 nm (calculated using the Scherrer formula).

TEM study

Fig. 2 shows transmission electron microscopy (TEM) images of as-prepared and calcined materials. Spherical or globular particles with sizes of 100–200 nm are present in as-prepared and calcined SMT. These particles are agglomerates of very small relatively monodispersed particles of about 10 nm in size [Fig. 2(B)], which is in good agreement with the XRD results. No discernible long-range order in the pore arrangement exists among the small particles. This is also confirmed by the absence of extra peaks in the low-angle XRD pattern. In fact, the pore packing motif can be reasonably described as "wormhole-like". In other words, the wormhole-like channels, which are more or less regular in diameter, are packed at random in the spherical or globular particles to form a three-dimensional mesoporous structure with a narrow pore size distribution. The regular separation between single channel walls may give rise to the low-angle XRD reflection. Similar disordered channel systems have been observed for disordered mesoporous silicas and aluminas.[3] The framework of SMT stays intact, even after calcination at 673 K [Fig. 2(C and D)]. This confirms the thermal stability of our mesoporous TiO_2.

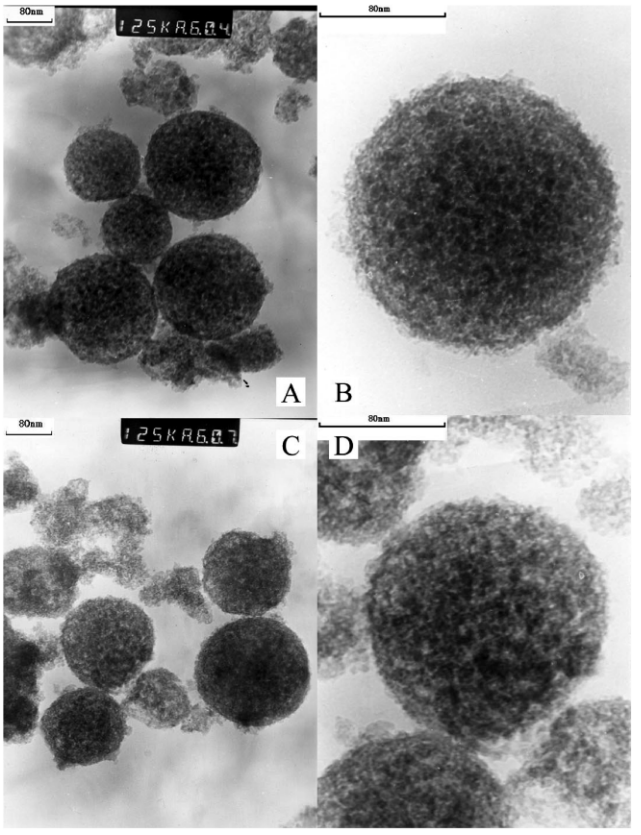

Fig. 2 TEM images of SMT-AP (A and B) and SMT-673 (C and D).

Nitrogen adsorption

The representative N_2 adsorption–desorption isotherm and Barrett–Joyner–Halenda (BJH) pore size distribution of calcined SMT are presented in Fig. 3. Both isotherms of as-prepared and calcined SMT have type H3 characteristics. The type H3 loop, which does not exhibit any limiting adsorption at high P/P_0, has been observed with aggregates of plate-like particles to give rise to slit-shaped pores.[17] The well-defined step in the adsorption isotherm and a hysteresis loop in the desorption isotherm between relative pressures P/P_0 of 0.45 to 0.9 are formed from the condensation of the adsorbate within the framework-confined mesopores.[18] The substantial hysteresis loop at high relative pressures above 0.9 is due to interparticle capillary condensation.[3] The interparticle pores can be seen in the TEM images (Fig. 2). The BET surface

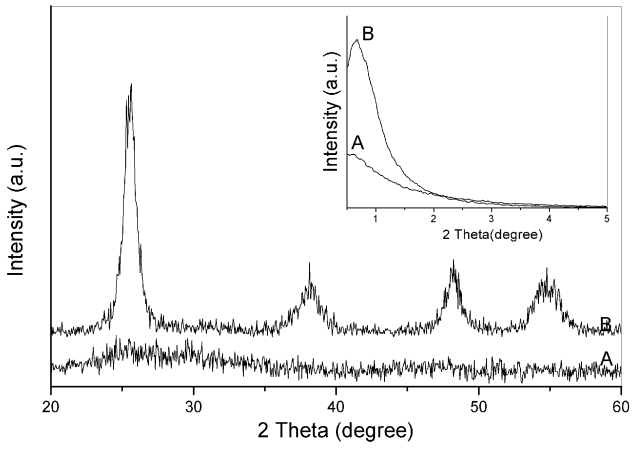

Fig. 1 Wide-angle and low-angle XRD patterns (inset) of as-prepared and calcined SMT. (A) SMT-AP, (B) SMT-673.

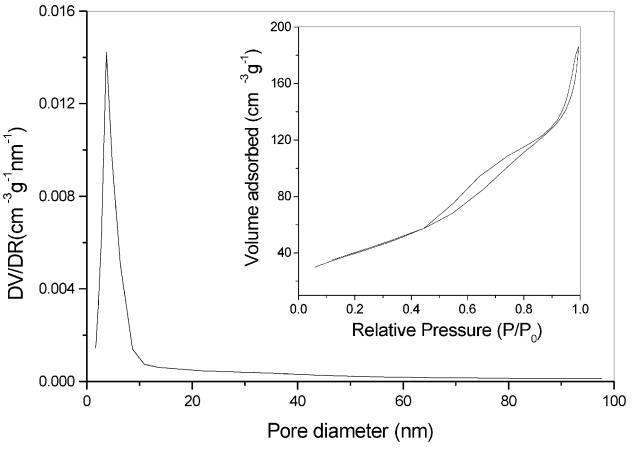

Fig. 3 N_2 adsorption–desorption isotherm (inset) and BJH pore size distribution plot for SMT-673.

area of SMT-AP is 487 m^2 g^{-1}, with a pore size of 4.0 nm (calculated using the BJH model) and a pore volume of 0.52 ml g^{-1} (single point total volume at $P/P_0 = 0.99$). The surface area of SMT-673 is 144 m^2 g^{-1}. N_2 adsorption results indicate that this material retains its mesoporosity, narrow pore size distribution and high surface area to at least 673 K. The pore size of SMT decreases slightly after calcination. The N_2 adsorption results further confirm the high thermal stability of SMT.

TGA/DTA study

Fig. 4 shows TGA and DTA curves for SMT-AP. The first weight loss of *ca.* 14% in the range 298–473 K, where there is an evident endothermic peak, is attributed to the loss of ethanol and adsorbed water. In the range 573–673 K, there is a second weight loss of about 3%, which corresponds to the condensation of hydroxyl groups linked to titanium.[19] The exothermic peak appearing around 633 K in the DTA curve is attributed to the crystallization of amorphous TiO_2. The total weight loss is only about 20%, which is much less than the 53% loss observed for the sonochemically prepared mesoporous TiO_2 synthesized using octadecylamine as a structure-directing agent.[19] In that preparation method, the octadecylamine alone would account for 27% of the total weight loss. The TGA/DTA results indicate that our ultrasound-induced agglomeration method is much more environmentally friendly.

FT-IR Spectroscopy

Fig. 5 shows the FT-IR spectra of SMT-673, SMT-AP and P25. All the spectra show one broad band around 3400 cm^{-1} and another around 1650 cm^{-1}. It has been reported that adsorbed water leads to bands around 3400 and 1630 cm^{-1},[20] while Ti–OH bonds produce absorbances around 3563, 3172, and 1600 cm^{-1},[21] Therefore, it is believed that the two peaks at 3400 and 1650 cm^{-1} correspond to surface-adsorbed water and hydroxyl groups.[22] As shown in Fig. 5, the SMT samples have more surface-adsorbed water and hydroxyl groups than P25, due to their larger surface areas. The peak around 2400 cm^{-1} comes from CO_2 in air. However, two extra peaks, assigned to a bidentate carboxylate ligand (COO^-), were observed in both SMT samples, which are due to the symmetric (~1450 cm^{-1}) and antisymmetric (~1580 cm^{-1}) stretching vibrations of carboxylic groups.[23] We conclude that the coordination structure between acetic acid and TIP is very stable, even after calcination at 673 K, a fact which was also recently noted by Takenaka *et al.*[24]

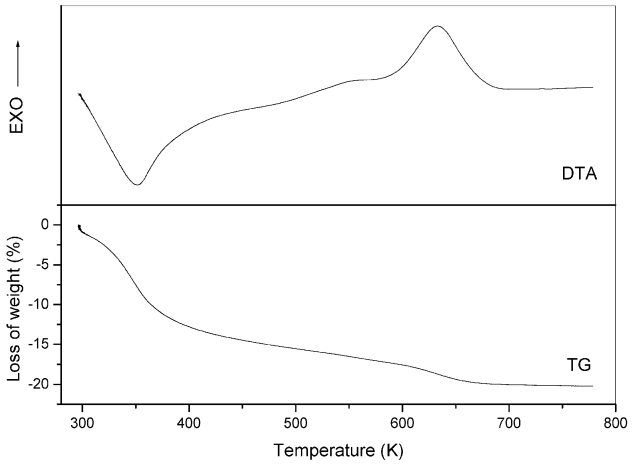

Fig. 4 TGA and DTA curves for SMT-AP.

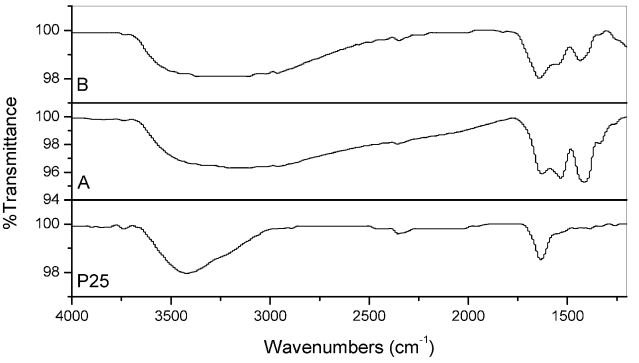

Fig. 5 FT-IR spectra of SMT-AP (A), SMT-673 (B) and P25.

Carboxylic acids with long alkyl chains can serve as surfactants to produce lamella-type mesophases in precursors by forming complexes with titanium alkoxide although the alkyl chain of acetic acid is too short to show surfactant characteristics, according to the results of Takenaka *et al.*[24] In their research, mesoporous titania was prepared from TIP and various carboxylic acids with different alkyl chain lengths [$CH_3(CH_2)_nCOOH$: $n = 0$–20]. A lamella-type mesophase was formed in the precursors when $n > 10$, while no peaks were observed in low-angle XRD patterns of samples prepared using carboxylic acids with $n < 10$. However, after calcination at 673 K, the peaks in the low-angle region assigned to the lamella phase also disappeared, even in samples from carboxylic acids with $n > 10$, while the peak due to SMT becomes stronger and more distinct. In our preparation approach, acetic acid is not only an acid catalyst, but also a ligand that changes the alkoxide precursor at a molecular level, thus modifying the whole hydrolysis condensation process.[25] Acetic acid can desirably slow down the rate of hydrolysis of TIP by forming $Ti(OPr^i)_x(OAc)_y$ compounds, because AcOH is negatively charged ($\delta_{AcOH} = -0.7$) while PrOH is positively charged ($\delta_{PrOH} = +0.1$). The PrOH molecule is a better leaving group, giving rise to $Ti(OPr^i)_x(OAc)_y$. When this new precursor is added into water, less electronegative alkoxide ligands are hydrolyzed preferentially, whereas more strongly bonded complexing groups are more difficult to remove. The remaining complexing groups behave as termination reagents, which decrease the tendency toward condensation. Uncontrolled precipitation is therefore avoided. Stöcker and Baiker prepared zirconia aerogels from tetra(*n*-butoxy)zirconium using different types of mono- and dicarboxylic acid catalysts.[26] In order to obtain mesoporous ZrO_2 with a high surface area, high temperature supercritical drying of the gels and careful thermal treatment (first heating in a nitrogen flow, then cooling in air flow) were necessary and the whole synthesis was very time-consuming. It is well known that high intensity ultrasound irradiation generates many localized hot spots, which can cause the homogeneous formation of a large number of seed nuclei.[10] Thus, monodispersed TiO_2 sol particles are formed very effectively under ultrasound irradiation when uncontrolled hydrolysis is avoided. It was reported that turbulent flow and shock waves produced by acoustic cavitation can drive metal particles together at high velocities.[27] A high speed collision can generate localized high temperature regions to enhance the condensation reactions among hydroxyl groups on adjacent TiO_2 sol particles.[28] The agglomerates thus formed are clearly shown in the TEM images. We believe that monodispersed TiO_2 sol particles are initially formed by ultrasound-assisted hydrolysis of acetic acid-modified TIP. Then, the mesoporous spherical or globular particles with a narrow pore size distribution are produced by controlled condensation and agglomeration of these sol nanoparticles under high intensity ultrasound irradiation. According to Prouzet and Pinnavaia,[29] if the *d*-spacing of the worm-like pore structure is assumed be

the average distance between channel centers, the average wall thickness can be deduced by subtracting the pore size from the *d*-spacing. Applying this assumption to calcined SMT, the wall thickness of SMT-673 is about 9.3 nm, which is about the same as the crystallite size (8.6 nm) calculated from the wide-angle XRD pattern. This result indicates that the mesoporous structure is produced by the agglomeration of TiO_2 nanoparticles. The high thermal stability of SMT is attributed to its thick and robust inorganic walls.

Photocatalytic activity for the oxidation of acetone in air

We investigated the photocatalytic activity of SMT for the oxidation of acetone in air. For comparison, commercial nanoparticulate TiO_2 (P25) with a high activity was also tested under identical conditions. Table 1 summarizes the properties and photocatalytic activity of SMT. As-prepared SMT has negligible activity due to its amorphous structure. After calcination, SMT shows better activity than P25. We attribute the high photocatalytic activity of calcined SMT to two reasons. The first is its high surface area, which increases the number of surface-adsorbed water and hydroxyl groups. It is well known that surface-adsorbed water and hydroxyl groups can react with photoexcited holes on the catalyst surface and produce hydroxyl radicals, which are powerful oxidants in degrading organics.[30] Secondly, the three-dimensional connectivity of mesoporous wormhole frameworks can promote the diffusion of reactants and products.[31] As the TEM images show, SMT has uniform mesopores that are three-dimensionally interconnected. This is very different from one-dimensional M41S. Although long-range ordered M41S materials are desirable for electronic and photonic applications where structural periodicity is important, the three-dimensional connectivity of mesoporous wormhole frameworks can reduce the diffusion limits of reactants and products and enhance the activity by facilitating access to reactive sites in the framework.[32]

In conclusion, highly active, three-dimensional, thermally stable mesoporous TiO_2 with a narrow pore size distribution has been synthesized by ultrasound-induced agglomeration (UIA) without the use of a template. This method is rapid and environmentally friendly. The high activity of calcined SMT is attributed to its high surface area and the three-dimensional connectivity of its mesoporous wormhole framework. We are currently working towards extending this method to the synthesis of other materials.

Experimental

Synthesis

Titanium isopropoxide (0.032 mol) and glacial acetic acid (0.016 mol) were dissolved in 20 ml absolute ethanol. After stirring for 1 h, the resulting solution was added drop by drop to 100 ml deionized water under sonication. During the whole process, the sonication cell was water-cooled to avoid overheating. The suspension was sonicated for 3 h (3 s on, 1 s off, amplitude 95%) using a 13 mm diameter high intensity probe (Sonics and Materials, VC750, 20 KHz). The powders were collected by centrifugation, washed with deionized water, and dried in an oven at 373 K. The as-prepared powder was calcined in air at 673 K for one hour to yield SMT-673.

Characterization

The low-angle and wide-angle powder X-ray diffraction (XRD) patterns were recorded on Rigaku D/MAX-RB and Philips MPD 18801 diffractometers, respectively, using Cu-Kα irradiation. HRTEM studies were carried out on a Philips CM-120 electron microscope. The samples for HRTEM were prepared by dispersing the final powders in ethanol; the dispersions were then dropped on carbon–copper grids. The nitrogen adsorption and desorption isotherms at 77 K were measured using a Micrometritics ASAP2000 system; samples were vacuum dried at 473 K overnight. TGA and DTA were performed using a Netzsch STA 409C thermal analyzer, under an air flow of 100 ml min^{-1} with a heating rate of 10 K min^{-1} from room temperature to 773 K. IR spectra of pellets of the samples mixed with KBr were recorded on a Nicolet Magna 560 FTIR spectrometer at a resolution of 4 cm^{-1}. The concentrations of the samples were kept around 0.25–0.3%.

Measurement of photocatalytic activity

The photocatalytic activity experiments on the mesoporous TiO_2 for the oxidation of acetone in air were performed at ambient temperature using a 7000 ml reactor. The photocatalysts were prepared by coating an aqueous suspension of mesoporous TiO_2 onto three dishes with diameters of 5.0 cm. The weight of the photocatalyst used for each experiment was set at 0.3 g. The dishes containing the photocatalyst were pretreated in an oven at 100 °C for 1 h and then cooled to room temperature before use.

After placing the dishes coated with the photocatalysts in the reactor, a small amount of acetone was injected with a syringe. The reactor was connected to a pump and a dryer containing $CaCl_2$ for adjusting the starting concentration of acetone and controlling the initial humidity in the reactor. The analysis of acetone, carbon dioxide and water vapor concentration in the reactor was performed with a Photoacoustic IR Multi-gas Monitor (INNOVA Air Tech Instruments model 1312). The acetone vapor was allowed to reach adsorption equilibrium with the photocatalyst in the reactor prior to experimentation. The initial concentration of acetone after the adsorption equilibrium was 400 ppm, which remained constant until a 15 W 365 nm UV lamp (Cole-Parmer Instrument Co.) in the reactor was turned on. The initial concentration of water vapor was 1.20 ± 0.01 vol%, and the initial temperature was 25 ± 1 °C.

Table 1 Summary of structure parameters and photocatalytic activities of as-prepared and calcined SMT

Material designation	BET surface area/m^2 g^{-1}	BJH pore diameter[a]/nm	*d*-spacing/nm	Wall thickness[b]/nm	Crystalline size[c]/nm	Degradation rate/ppm min^{-1} g^{-1}
SMT-AP	487	4.0	15	11	—	Negligible
SMT-673	144	3.7	13	9.3	8.6	3.72
P25	50	—	—	—	23.7	3.11

[a] Mesopore diameter at maximum peak estimated using the BJH model from the adsorption branch of the isotherm. [b] Deduced by subtracting the pore size from the *d*-spacing. [c] Calculated using the Scherrer formula from the wide-angle XRD patterns.

Acknowledgements

The work described in this paper was partially supported by a grant from the National Natural Science Foundation of China and the Research Grants Council of the Hong Kong Special Administrative Region, China (project no. N-CUHK 433/00). We thank Prof. Guoqing Xiong, Dalian Institute of Chemical Physics, for helpful discussions.

References

1 C. T. Kresge, M. E. Leonowicz, W. J. Roth, J. C. Vartuli and J. S. Beck, *Nature*, 1992, **359**, 710.
2 D. M. Antonelli and J. Y. Ying, *Angew. Chem., Int. Ed. Engl.*, 1995, **34**, 2014.
3 (*a*) P. T. Tanev and T. J. Pinnavaia, *Science*, 1995, **267**, 865; (*b*) S. A. Bagshaw, E. Prouzet and T. J. Pinnavia, *Science*, 1995, **269**, 1242; (*c*) S. A. Bagshaw and T. J. Pinnavia, *Angew. Chem., Int. Ed. Engl.*, 1996, **35**, 1102.
4 Y. Wei, D. L. Jin, T. Z. Ding, W. H. Shih, X. H. Liu, S. Z. D. Cheng and Q. Fu, *Adv. Mater.*, 1998, **10**, 313.
5 J. B. Pang, K.Y. Qiu, Y. Wei, X. J. Lei and Z. F. Liu, *Chem. Commun.*, 2000, 477.
6 J. B. Pang, K.Y. Qiu and Y. Wei, *J. Non-Cryst. Solids*, 2001, **283**, 101.
7 J. C. Jansen, Z. Shan, L. Marchese, W. Zhou, N. von der Puil and T. Maschmeyer, *Chem. Commun.*, 2001, 713.
8 J. Lin, J. C. Yu, D. Lo and S. K. Lam, *J. Catal.*, 1999, **183**, 368.
9 P. D. Yang, D. Y. Zhao, D. I. Margolese, B. F. Chmelka and G. D. Stucky, *Chem. Mater.*, 1999, **11**, 2813.
10 P. Kluson, P. Kacer, T. Cajthaml and M. Kalaji, *J. Mater. Chem.*, 2000, **11**, 644.
11 K. S. Suslick, S. B. Choe, A. A. Cichowlas and M. W. Grinstaff, *Nature*, 1991, **353**, 414.
12 K. S. Suslick and G. J. Price, *Annu. Rev. Mater. Sci.*, 1999, **29**, 295.
13 Y. Q. Wang, X. H. Tang, L. X. Yin, W. P. Huang, Y. R. Hacohen and A. Gedanken, *Adv. Mater.*, 2000, **12**, 1183.
14 W. P. Huang, X. H. Tang, Y. Q. Wang, Y. Koltypin and A. Gedanken, *Chem. Commun.*, 2000, 1415.
15 C. Y. Chen, H. Y. Li and M. E. Davis, *Microporous Mater.*, 1993, **2**, 17.
16 Q. S. Huo, D. I. Margolese, U. Ciesla, D.G. Demuth, P. Y. Feng, T. E. Gier, P. Sieger, A. Firouzi, B. F. Chmelka, F. Schüth and G. D. Stucky, *Chem. Mater.*, 1994, **6**, 1176.
17 K. S. W. Sing, D. H. Everett, R. A. W. Haul, L. Moscou, R. A. Pierotti, J. Rouquerol and T. Siemieniewska, *Pure Appl. Chem.*, 1985, **57**, 603.
18 P. J. Branton, P. G. Hall, K. S. W. Sing, H. Reichert, F. Schüth and K. K. Unger, *J. Chem. Soc., Faraday Trans.*, 1994, **90**, 2965.
19 Y. Q. Wang, S. G. Chen, X. H. Tang, O. Palchik, A. Zaban, Y. Koltypin and A. Gedanken, *J. Mater. Chem.*, 2001, **11**, 521.
20 T. Nakayama *J. Electrochem. Soc.*, 1994, **141**, 237.
21 E. Sanchez, T. Lopez, R. Gomez, X. Bokhimi, A. Morales and O. Novaro, *J. Solid State Chem.*, 1996, **122**, 309.
22 Z. Ding, G. Q. Lu and P. F. Greenfield, *J. Phys. Chem. B*, 2000, **104**, 4815.
23 C. J. Brinker and G. W. Schere, *Sol–Gel Science, the Physics and Chemistry of Sol–Gel Processing*, Academic Press, Boston, MA, 1990.
24 S. Takenaka, R. Takahashi, S. Sato and T. Sodesawa, *J. Sol–Gel Sci. Technol.*, 2000, **19**, 711.
25 J. Livage and C. Sanchez, *J. Non-Cryst. Solids*, 1992, **145**, 11.
26 C. Stöcker and A. Baiker, *J. Sol–Gel Sci. Technol.*, 1997, **10**, 269.
27 S. J. Doktycz and K. S. Suslick, *Science*, 1990, **247**, 1067.
28 S. Ramesh, Y. Koltypin and A. Gedanken, *J. Mater. Sci.*, 1997, **12**, 3271.
29 E. Prouzet and T. J. Pinnavaia, *Angew. Chem., Int. Ed. Engl.*, 1997, **36**, 516.
30 C. S. Turchi and D. F. Ollis, *J. Catal.*, 1990, **122**, 178.
31 J. C. Yu, J. G. Yu, W. K. Ho and L. Z. Zhang, *Chem. Commun.*, 2001, 1942.
32 Z. Shan, E. Gianotti, J. C. Jansen, J. A. Peters, L. Marchese and T. Maschmeyer, *Chem. Eur. J.*, 2001, **7**, 1437.